NON-DESTRUCTIVE EVALUATION OF ADDITIVELY MANUFACTURED PARTS VIA IMPEDANCE-BASED MONITORING

Mohammed Albakri[1], Logan Sturm[2], Christopher B. Williams[2], Pablo Tarazaga[1]

[1] Vibrations, Adaptive Structures, and Testing Laboratory
[2] Design, Research, and Education for Additive Manufacturing Systems Laboratory
Department of Mechanical Engineering; Virginia Tech

ABSTRACT

The ability of Additive Manufacturing (AM) processes to fabricate complex geometries is somewhat hindered by an inability to effectively validate the quality of printed complex parts. Furthermore, there are classes of part defects that are unique to AM that cannot be efficiently measured with standard Quality Control (QC) techniques (e.g., internal porosity). Current QC methods for AM are limited to either destructive evaluation of printed test coupons, or expensive radiation-based scanners of printed parts for non-destructive evaluation. In this paper, the authors describe their use of impedance-based structural monitoring to indirectly measure printed part abnormalities. By bonding a piezoceramic (PZT) sensor to a printed part, the measured electrical impedance of the PZT can be directly linked to the mechanical impedance of the part. By observing deviations in the mechanical impedance of the part, as determined by this quick, non-intrusive electrical measurement, one is able to detect the existence of part defects. In this paper, the authors explore the effectiveness and sensitivity of the technique as a means for detecting of a variety of defect types and magnitudes.

1. NON-DESTRUCTIVE EVALUATION FOR ADDITIVE MANUFACTURING

1.1. Challenges of Quality Control for Additively Manufactured Parts
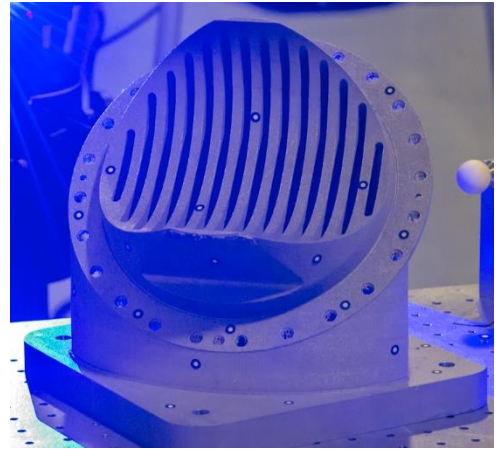
As Additive Manufacturing (AM) technologies and materials continue to mature, there has been a sudden and significant increase in the amount of end-use products fabricated via AM. AM technologies' layerwise approach to fabrication provides designers opportunities to realize products that feature complex geometries that can be tailored to simultaneously meet several design objectives and functionalities. These advances have been observed predominately in the aerospace industry where highly valued, highly engineered, and customized products are produced in low volumes, which fits well with current economic justifications for AM implementation. Some of the notable applications of direct-metal AM technologies to fabricate end-use products include GE Aviation's LEAP 56 fuel nozzle (Figure 1a), SpaceX's SuperDraco combustion chamber for the Dragon V2 rocket engine (Figure 1b), and various rocket components for NASA including a Pogo-Z baffle for RS-25 engine (Figure 1c).

(a) GE fuel nozzle [1]   (b) SpaceX combustion
                               chamber [2]   (c) NASA engine baffle [3]

Figure 1. Example applications of AM to fabricate mission-critical aerospace products

While efforts in employing AM technology to produce mission-critical parts are rapidly advancing, research and development of quality control techniques to validate these parts is lacking. Perhaps ironically, the challenges in qualification of AM stem from the complexity that AM offers to designers. Complex geometries that contain inaccessible features (e.g., internal channels) cannot be quickly measured for using conventional metrology techniques. This, alogn with the frequent occurrence of deeply embedded flaws (e.g., internal porosity and cracks) in direct-metal Powder Bed Fusion processes, require non-destructive evaluation (NDE) techniques for part qualification.

However, current NDE techniques are not readily suitable for analysis of AM parts. Dimensional measurement techniques such as Coordinate Measuring Machines (CMM) and Structured Light (SL) scanning require access to all surfaces of the part, which is not always certain given the design freedoms offered by AM. While Eddy Current Testing (ECT) and Ultrasonic Testing (UT) techniques can been used to detect internal porosity, their application to AM parts is limited as they must have access to all surfaces, they have limited surface penetration, and they are sensitive to surface roughness. While Penetrant Testing and Magnetic Particle Testing techniques are less geometry-sensitive, they could not be employed to assess parts featuring internal structures.

Computed tomography (CT) is currently the NDE technique most often used to inspect AM parts as it can readily inspect the entirety of a part, regardless of its geometry and internal structure. CT has been demonstrated by NASA to detect deep/embedded defects, interrogate inaccessible features, and to characterize and qualify as-manufactured AM parts [4]. However, there are some limitations to the use of CT as a means for inspecting AM parts. It is costly and time-intensive. It is not able to reliably detect cracks that are oriented perpendicular to the x-ray beam may not be detected. There exists also a trade-off in penetration depth and the resolution of the inspection,

which could result in a failure of identifying deeply embedded micro-porosity. Also, larger parts are pushing the physical limits of the existing CT systems.

1.2. Non-Destructive Evaluation for Additive Manufacturing

In their *Measurement Science Roadmap for Metal-based Additive Manufacturing*, NIST states that "Existing NDE techniques are not optimized for AM processes, materials or parts. Techniques are lacking for in-situ NDI, and post-process AM part inspection." The authors suggest that an ideal post-process NDE technique for AM would have the following attributes:

- Cost-effective
- Able to conducted quickly; preferably in-line during post-processing
- Able to evaluate a part irrespective of geometry, surface, and material. I.e., the technique would be able to analyze inaccessible features, large parts, fine features, rough surface finish, etc.
- Able to detect typical AM build errors including feature location deviation, feature size (part mass deviation), and deeply embedded flaws.

In addition to these requirements, the authors suggest that an ideal NDE technique would be free of cyber-physical vulnerabilities. As discussed in their previous work [5], the authors suggest several cyber-physical security vulnerabilities in AM and in quality control due to the reliance of digital files throughout the process chain (CAD file, STL file, toolpath file, AM machine firmware, and even the output of the metrology system), which can be easily altered by an attacker. Thus, an ideal NDE technique would be separate from the system and part data, and instead treated as a second-channel measurement of the AM process's functionality.

In this regard, an ideal AM NDE technique would resemble existing functional testing schema for evaluating Printed Circuit Boards (PCBs). When PCBs are qualified, one doesn't test the connectivity of every solder point on the board or the tolerance of the part placement. Instead, one tests the functionality of the PCB by placing an input voltage into the board and measures its functional response. This type of in-line go or no-go decision making is ideal for a post-process NDE technique as it is cost-effective, quick, and is cyber-secure.

1.3. Research Goal

The lack of reliable means for verifying the quality of a printed part is a significant barrier to further industrial adoption of AM technologies. Without a means of performing part validation and certification, it is not possible to specify the use of AM for the fabrication of a mission-critical part. As such, the need for creating NDE techniques that are optimized for AM has been identified as a research area of critical importance by several organizations such as NIST [6], NASA [4], and the ASTM F-42 committee [7]. Due to the established deficiencies of existing NDE techniques, NIST's roadmap action plan suggests that the community conducts research and development for new post-process NDE techniques that are optimized for AM.

To address this research gap, the authors propose to use impedance-based Structural Health Monitoring (SHM) as a means to identify part defects. In SHM, a pizeoceramic (PZT) sensor is bonded to a printed part and excited across a range of frequencies. Due to the coupled

electromechanical characteristics of the PZT, the electrical impedance of the piezoelectric sensor can be related to the mechanical impedance of the part, thus allowing for indirect measurements of a part's mass, stiffness, and damping (which are directly related to the part mass and structure). It is hypothesized that this quick, non-intrusive electrical measurement will allow for observiation of part deviations when compared to measurement of an equivalent baseline, defect-free part. A detailed overview of the impedance-based SHM technique is provided in Section 2.

The overall goal of this paper is to demonstrate and assess the feasibility/usefulness of SHM as a means of NDE of additively manufactured parts. This research is guided by two primary research questions: "What types of defects can a SHM technique detect?" and "What defect magnitudes can it detect?" To answer these questions, the authors design and print a series of test specimens which contain build errors typical of AM processes (Section 3.1). SHM measurements are conducted and compared against a pair of baseline parts (Section 3.2-3.4). Results from this comparison are presented and analyzed in Section 4. Closure and future work are presented in Section 5.

2. IMPEDANCE-BASED STRUCTURAL MONITORING

The fundamental basis of most damage identification methods is that the presence of damage will alter the mass, stiffness and damping characteristics of the structure, which in turn reflect on the measured dynamic response. Among the different SHM techniques, impedance-based SHM has emerged as a promising, non-intrusive, cost-effective, highly-sensitive solution for real-time damage assessment [8]. This technique utilizes piezoelectric materials, lead zirconate titanate (PZT) wafers in particular, as collocated sensors and actuators to simultaneously excite the structure and measure its response [9, 10]. Making use of the coupled electromechanical behavior of piezoelectric materials, the problem of measuring the mechanical impedance of the host structure is significantly simplified, and it is directly related to the electrical impedance of the piezoelectric active sensors. Therefore, changes in the host structure induced by printing defects are reflected on the electrical impedance of the piezoelectric sensors, and thus, can be detected.

Figure 2 shows a schematic of a piezoelectric patch attached to a printed part, which is represented by a spring, mass, and damper system.
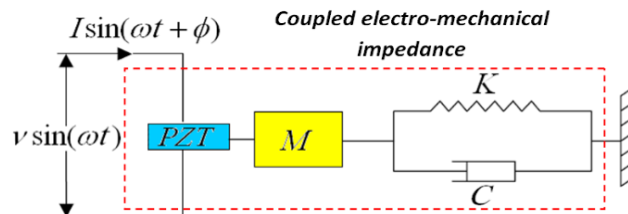
Figure 2. A piezoelectric patch attached to a mechanical structure represented by a spring-mass-damper system.

Assuming linear piezoelectricity, the constitutive equations of the piezoelectric materials operating in 1-3 mode are [11]:

$$\varepsilon_{11} = d_{13}E_3 + \overline{s}_{11}^E \sigma_{11}$$
$$D_3 = \overline{e}_{33}^\sigma E_3 + d_{31}\sigma_{11}$$

Eq.1

where ε_{11} is the mechanical strain, σ_{11} is the stress, D_3 is the electric displacement, E_3 is the electric field, d_{31} is the piezoelectric coupling coefficient, $\overline{s}_{11}^E = s_{11}^E(1-i\eta)$ is the complex mechanical compliance of the material measured at zero electric field, $\overline{e}_{33}^\sigma = e_{33}^\sigma(1-i\delta)$ is the complex permittivity measured at zero stress, and η and δ are the mechanical loss factor, and the dielectric loss factor, respectively.

Due to the coupled electromechanical behavior of piezoelectric materials, the electrical impedance of the piezoelectric sensors is directly related to the mechanical impedance of the host structure, $Z_{Structure}$, as follows [9]:

$$Z(\omega) = \frac{V}{I} = -i\frac{h}{\omega wl}\left[\overline{e}_{33} - d_{31}^2\overline{s}_{11}^E + \frac{Z_{PZT}}{Z_{Structure}+Z_{PZT}}d_{31}^2\overline{s}_{11}^E\frac{\tan(kl)}{kl}\right]^{-1}$$

Eq. 2

where $Z_{PZT} = -i\frac{wh\overline{s}_{11}^E}{\omega l}\cdot\frac{kl}{\tan(kl)}$ is the piezoelectric sensor short circuit impedance, $k = \left(\omega^2\rho/\overline{s}_{11}^E\right)^{1/2}$ is the wave number, ρ is the density of the piezoelectric material, w, h, and $2l$ are the piezoelectric patch width, thickness and length, respectively.

Being a vibration-based damage identification technique, the sensitivity of impedance-based SHM depends on the frequency range at which the structure is excited and response is measured. It has been shown that the wavelength of the excitation signal has to be smaller than the characteristic length of the damage in order for it to be successfully detected [12]. Therefore, for enhanced sensitivity, impedance-based SHM is carried out at high frequencies.

Peairs et al. [13] studied the possibility of preselecting preferred frequency ranges based on the free transducer characteristics. They concluded that the characteristics of the both the transducer and the structure to be monitored determine the optimal monitoring frequency ranges.

Impedance-based SHM has been successfully applied to detect damage in numerous civil, aerospace, and mechanical components and structures. Park et al. [14] successfully implemented this technique for real-time damage detection in composite reinforced concrete walls, a bridge section, and a pipe joint. Several other studies presented the successful implementation of impedance-based SHM to detect structural defects in laboratory environment and under real operating conditions.

The authors hypothesize that this technique is especially relevant and appropriate for inspection of AM parts as it fits many of the needs identified in Section 1.2. The technique is cost-effective (i.e., no radiation source is needed) and the analysis (i.e., a full sweep across all frequencies of interest) can be completed in less than 30 seconds. The high-frequency technique can be used to detect internal damage throughout the part without the need for access to all points on a part's surface, and is thus applicable for inspecting parts with complex geometries. Fundamentally, SHM is a functional measurement of the physical properties (mass, stiffness, damping) of a part. As these three physical properties will always differ between a defect-free part

and a damaged part, SHM should be able to effectively detect all types of manufacturing defects with a single measurement.

3. EXPERIMENTAL METHODS

3.1. Test Specimen Design

To evaluate the effectiveness of the impedance-based measurement technique as a means of inspecting AM parts, the authors sought to design a test part that can replicate common types of errors that can occur in parts fabricated using AM. The authors identified three types of generalized build errors common in all AM technologies:

1. *Dimensional inaccuracies*: These errors, in which the finished part has an incorrect final mass, can occur when either too much or too little material is deposited/fused/cured. This can occur if the machine is not properly configured or calibrated; e.g., the feed rate of an extrusion nozzle is too high, the laser power is too high, the droplet saturation level is too high, etc. This error can also occur due to machine failure; e.g., a misfire of a jetting nozzle, a clogged extrusion nozzle, poorly formed powder bed layer, etc. While the exact cause of excess/lack of material will vary process to process, the resulting error can occur across all AM processes.
2. *Positional inaccuracies*: These types of errors, in which the final part has the correct final mass but the deposited/formed mass is not accurately positioned, can be caused by improper machine calibration or machine error. This can occur if the stages' motors are not properly zeroed, there is an error in the toolpath file, the part warps during/after the build, etc.
3. *Internal porosity*: This type error refers to gaps or voids that are formed in the internal structure of a part during its build. This can occur due to process errors that result in a reduced melt pool size, incorrect tool path file, and can even be intentionally caused by a cyber-physical attack [5].This type of defect is unique to AM systems when compared to traditional subtractive manufacturing techniques. It differs from the above two presented build error as it represents a loss of model material that is completely enclosed inside the part (thus preventing direct measurement with a device such as calipers). This error is difficult to detect not only because it is within the part structure, but also because, depending on the nature of the AM process in question, this void may often be filled with unhardened model material or supporting material. The presence of this support material may result in the void having little to no effect on the mass of part while significantly reducing its strength.

The authors' goal was to design a test part that allowed systematic analysis of the SHM technique's ability to evaluate each of three build errors typologies identified. In addition, the design of the test part was guided by the following additional considerations:

- The part should allow for multiple defect types to be combined to enable examination of the effects of their interaction.

- The test part should allow the magnitude (i.e., overall size) of the defects to be easily varied. This will allow the researchers to identify the minimum size of defect that can be determined.
- The part should contain geometric complexity to replicate conditions that cannot be inspected with traditional NDE techniques. However, the geometry should be sufficiently simple so that a substantial number of features can be measured efficiently to validate the overall print accuracy.
- The geometry should be designed such that the probability of process-imposed defect (i.e., part warping) is minimized.
- The part should be able to be printed quickly without excessive material consumption.

The resulting test part design is shown in Figure 3. The part, which measures 35mm x 35mm x 16mm, represents a trussed topology consisting of nine "pillars" and two "layers".
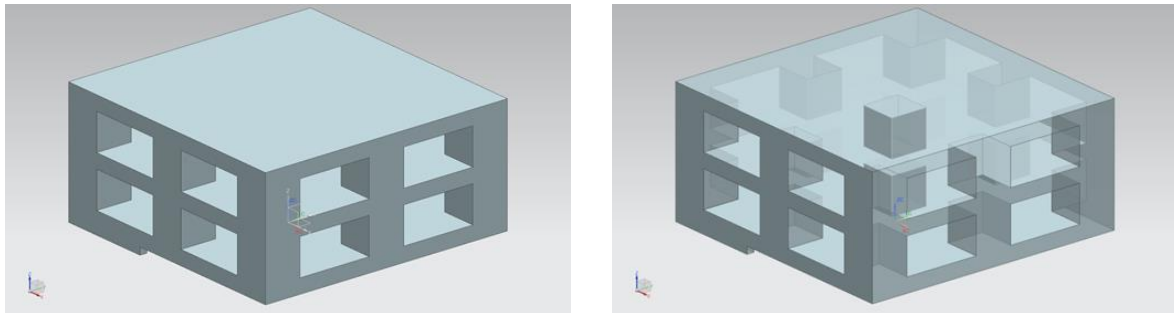

Figure 3. Test part consisting of nine pillars and two layers. On the left is the solid model; on the right is a transparent render of the part. The bottom feature is used to align the sensor.

The pillars allow different defects to be introduced in a variety of locations and manners. Pillars can be increased in size to change part mass and cause dimensional inaccuracies (Figure 4a and 4b), moved to create positional inaccuracies (Figure 4c), or have voids placed inside of them to create build defects (Figure 4d-f). The part also included a small 1mm tall feature on the bottom plate, which was used to quickly and consistently align the sensors across all specimens.

In addition to two unmodified control samples (used to establish a baseline response), a total of six test parts featuring varying build defects were created (Figure 4):

A. A part with a 1% total mass increase (made by widening the central pillar)
B. A part with a 5% total mass increase (made by widening the central pillar)
C. A part with the center pillar moved 1mm diagonally away from the sensor
D. A part with a 1mm^3 cubic void placed in the center pillar (0.0104% of total volume)
E. A part with a 8mm^3 cubic void placed in the center pillar (0.0831% of total volume)
F. A part with a 8mm^3 cubic void placed in the pillar in the far corner from the sensor

The defects in these specimens were chosen as they allowed the researchers to evaluate the SHM technique's ability to detect all defect types and its sensitivity to defect magnitude and location relative to the sensor.
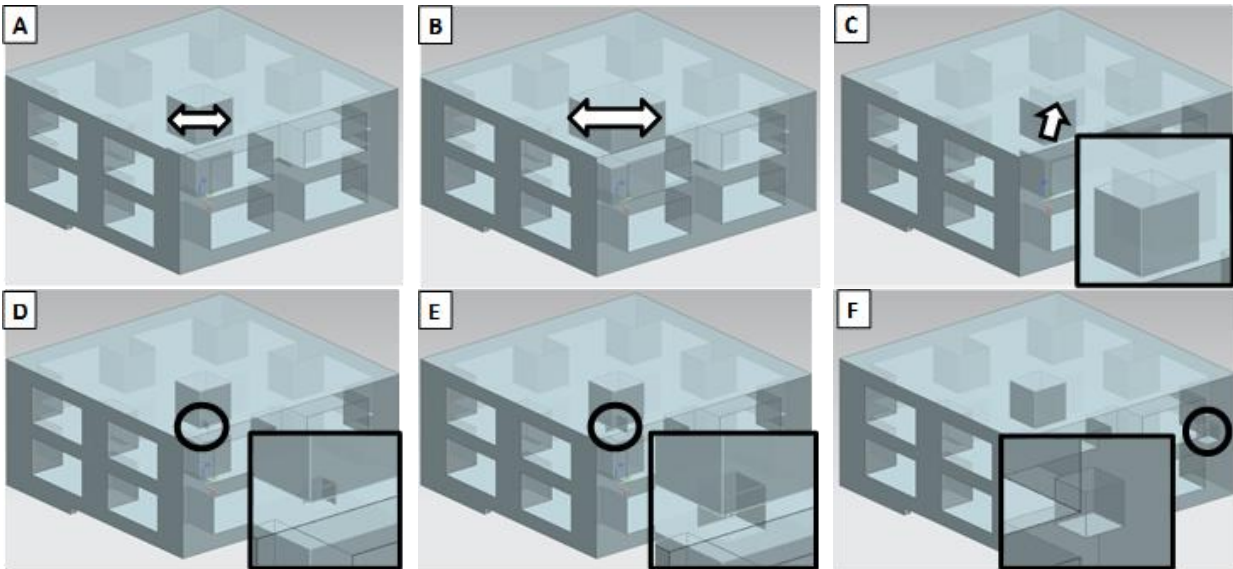
Figure 4. Tested defects; a) A 1% mass increase of the part by increasing the center pillar size, b) A 5% mass increase of the part by increasing the center pillar size, c) Movement of the center pillar by 1mm diagonally, d) A $1mm^3$ void placed in the center pillar, e) A $8mm^3$ void placed in the center pillar, f) A $8mm^3$ void placed in the corner pillar.

3.2. Test Specimen Fabrication

Each specimen was fabricated in VeroWhitePlus (a stiff acrylate photopolymer) using a Stratasys Connex 350 multi-material jetting AM system. As it was hypothesized that the sensitivity of the measurement technique would be affected by the resonance of the material, VeroWhitePlus was chosen since it was the stiffest material available to the researchers.

3.3. Impedance-based Measurements

Once printed, piezoceramic active sensors were attached to each of the test specimens. All piezoelectric patches were diced out of the same piezoelectric wafer to a shape of 0.5 in. × 0.5 in.. Superglue was used to bond the piezoelectric patches to the test parts. Figure 5a shows the eight test parts after bonding the piezoelectric patches.

In order to minimize the uncertainty associated with the bonding process, the raised edges integrated in the part design (Section 3.1), are used to guide the process of sensor placement. In this manner, all piezoelectric active sensors are placed at the same location, which makes the comparison between impedance signatures obtained from different parts valid. Minor variations due to bonding process imperfections are accounted for when defining damage metrics thresholds, as discussed in later sections.

For each part, impedance signature is measured using KEYSIGHT E4990A impedance analyzer. The frequency range selected for this experiment is 10-20 KHz, where frequency sweep is performed with 10 Hz resolution. The analyzer excites the piezoelectric patches with a 1 V peak-to-peak sinusoidal signal, and allows the structure to settle before measuring its response. To minimize the effects of noise, eight measurements are made and averaged at each frequency step. Figure 5b shows one of the test parts connected to the impedance analyzer during the test.
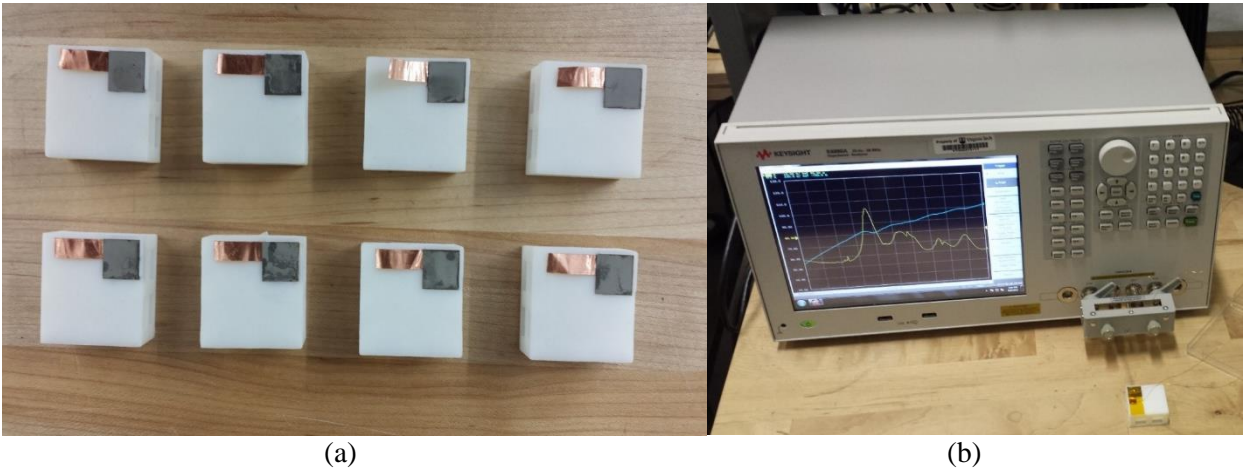
Figure 5. (a) Printed test parts with piezoelectric active sensors attached to them, and (b) KEYSIGHT E4990A impedance analyzer measuring the impedance signature of one part.

3.4. Damage Detection and Measurement Analysis

Impedance-based SHM can be used in either supervised or unsupervised learning constructs. In unsupervised learning, the analysis technique can be applied to an unknown set of parts and the damaged part(s) can be identified by analyzing the differences across all response signals. Alternatively, in a supervised learning approach, one compares differences in the electrical impedance of fabricated parts against a baseline signature from a known, defect-free part.

In this study, the authors situated the analysis in a supervised learning context: two parts were first fabricated and known to be defect free (Section 3.1). These parts are used to establish a baseline signature to which all other parts are compared. The impedance signature baseline is obtained by averaging the impedance signatures of the two defect-free control parts. Only the real part of the measured impedance is considered in this study, since it is known to be more sensitive to the mechanical characteristics of the host structure. The presence of printing defects in the other fabricated samples changes the mechanical impedance of the part, which in turn is reflected on the measured impedance signature. Therefore, changes in one part's impedance signature impedance compared to the baseline signature can be used as an indicator of printing defects.

To compensate for inconsistency in connectors' resistivity, due to soldering, copper tape, and wire length variations, all impedance signatures are shifted vertically such that their values at the lower end of the frequency range match. Only those features known to be sensitive to structural defects, such as shifts in peaks frequency, are utilized to indicate damage.

In order to quantify the variations in the impedance signature associated with each defect, two damage metrics are calculated. The first is based on the Root Mean Square Deviation (RMSD) definition, commonly used with impedance-based SHM. This is defined as follows:

$$RMSD = \sqrt{\sum \frac{(Z_D - Z_{BL})^2}{Z_{BL}^2}}$$

Eq. 3

where Z_D is the real component of the impedance signature of the part being tested, and Z_{BL} is the baseline impedance signature.

Another damage metric based on the correlation coefficient is defined according to the following equation:

<div align="right">Eq.4</div>

$$r = 1 - \left| \frac{n \sum Z_D Z_{BL} - \sum Z_D \sum Z_{BL}}{\sqrt{[n \sum Z_D^2 - (\sum Z_D)^2][n \sum Z_{BL}^2 - (\sum Z_{BL})^2]}} \right|$$

where Z_D and Z_{BL} follow the same definitions for Eq. 3, and n is the total number of points in each signature. Following this definition, the values of this damage metric ranges from zero, when the two signatures are matching perfectly, and 1, when there is no correlation between the current measurement and the baseline.

4. RESULTS AND DISCUSSION

4.1. Establishing Baseline Measurement

As described in Section 3.4, a baseline signature was first established by measuring the electrical impedance of two printed defect-free parts. Figure 6 shows the real part of the two impedance signatures along with the averaged response.
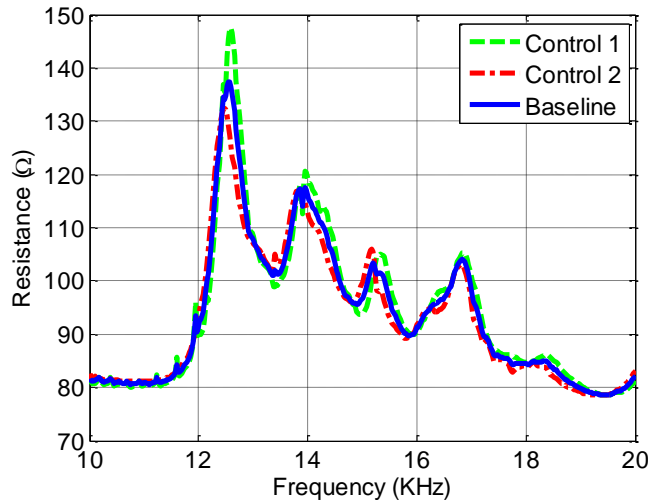

Figure 6. Real component of the impedance signatures of the two defect-free (control) parts, along with the baseline signature.

It is noticed that the two signatures are very close; however, imperfections in both printing and piezoelectric bonding processes result in minor discrepancies between the defect-free signatures. Such discrepancy in the control parts' impedance signatures will be used later to define damage detection threshold.

It is noted that it is only assumed that the parts are both free of defects. Measurements of the parts' masses and the dimensional accuracy of their accessible features. In practice, following the initial SHM measurement, one would first insure that the baseline part was defect free via a combination of additional NDE techniques and microscopy of a series of sectioned surfaces.

4.2. Effects of Dimensional Inaccuracy

As described in Section 3.1, dimensional inaccuracies are represented by changes in the overall part mass due to printer malfunction and/or incorrect process parameters. In this study, two parts – one featuring a 1% increase in mass, and another featuring a 5% increase in mass – were designed and fabricated to simulate this build error. In both parts, the mass increase was applied to the central "pillar" (Figure 4a and 4b). These errors were readily detected by the SHM technique, as seen by comparing their measured impedance signatures with those from the baseline signature (Figure 7).
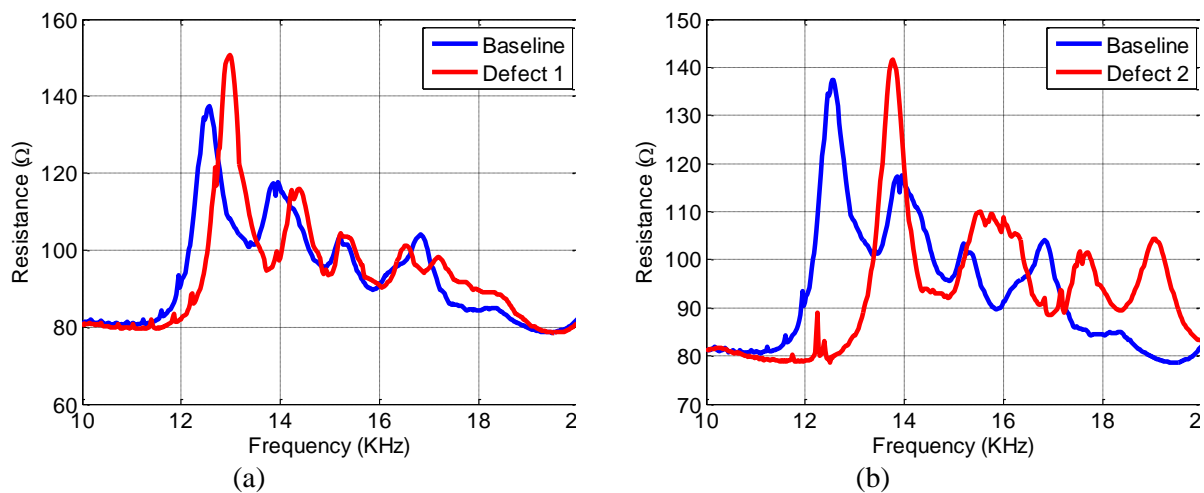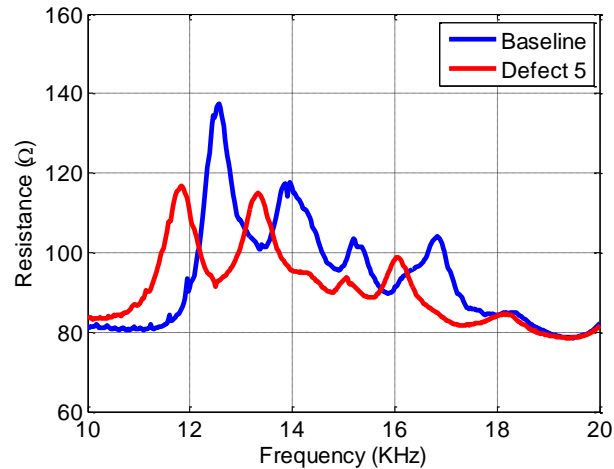

Figure 7. Impedance signatures for the defected parts compared to the baseline signature, (a) 1% mass increase by widening the central pillar, (b) 5% mass increase by widening the central pillar

As the central pillar is widened to simulate a mass increase, the peaks of the impedance signature are found to shift to the right, indicating an increase in the overall stiffness of the structure. This indicates that the resulting increase in the pillars stiffness - resulting from widening it - dominates the effect of added mass. As more mass is added, the shift in impedance peaks is found to increase.

4.3. Effects of Positional Inaccuracy

As indicated in Section 3.1, positional inaccuracy (in which part mass remains equivalent to the baseline, but its location is different) was simulated in the test part by shifting the central pillar away from the sensor by 1mm. The resulting impedance signature is shown in Figure 8 along with the baseline signature for comparison. As can be observed, the defect is found to introduce a significant change in the impedance signature over the selected frequency range.
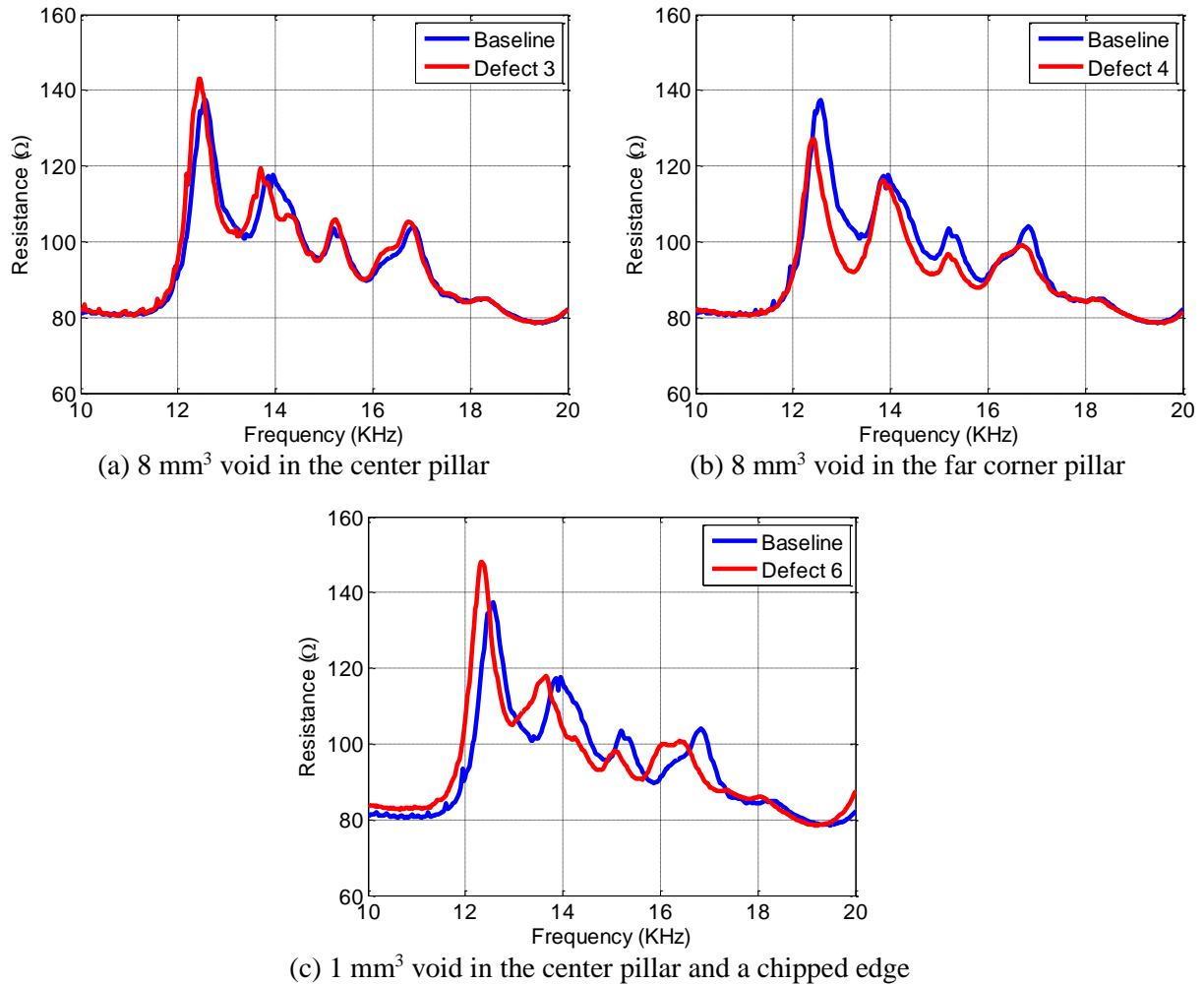
Figure 8. Impedance signatures for a 1mm displacement of the center pillar compared to the baseline signature

4.4. Effects of Internal Porosity

To analyze the SHM technique's capability to detect internal porosity, three test specimens were designed and printed (Section 3.1; Figure 4d-f). The impedance signatures for the three specimens (8 mm^3 void in the center pillar, 8 mm^3 void in the far corner pillar, 1 mm^3 void in the center pillar) are presented, along with the baseline signature for comparison, in Figure 9.

It is observed that that the impedance signatures of the void defects can be hardly distinguished from the baseline measurement, especially in the case of the 8 mm^3 void in the center pillar. It is noted that the 1 mm^3 void has a larger variation (Figure 9c); however, the part also had a small defect (mass loss) on its edge due the part being accidentally dropped during testing.

Unlike the cases of mass increase, where defects were easily detected, voids defects seem to have a smaller impact on the dynamic response in the selected frequency range. This is partly due to the fact that these voids are not hollow, but are rather filled with the PolyJet support material, which has a gel-like consistency that dampens vibrations. Further investigations are needed to study the effect of voids on impedance signatures, which is expected to be dependent on the frequency range over which the response is measures, the location of the void, along with its size.

(a) 8 mm³ void in the center pillar

(b) 8 mm³ void in the far corner pillar

(c) 1 mm³ void in the center pillar and a chipped edge

**Figure 9.** Impedance signatures for the parts featuring internal porosity

4.5. Analysis of Results

As noted in Section 3.4, two damage metric definitions (Root Mean Square Deviation and correlation coefficient) were used to quantify the variations in the impedance signature associated with each defect. The results of the RMSD analysis are shown in Figure 10a; the results from the correlation coefficient measurement are shown in Figure 10b.

Following both definitions, it is noted that damage metric values for the mass increase defects (Figure 7; Defects 1 and 2 in Figure 10), the mass decrease defects (caused by the chip in the part; Defect 6 in Figure 10 and Figure 9c), and the feature displacement defect (Figure 8; Defect 5 in Figure 10) are considerably larger than the defect-free parts (Figure 6; Control 1 and 2 in Figure 10). Thus, it can be concluded that such defects can be detected with high confidence using the proposed technique (in VeroWhitePlus material).
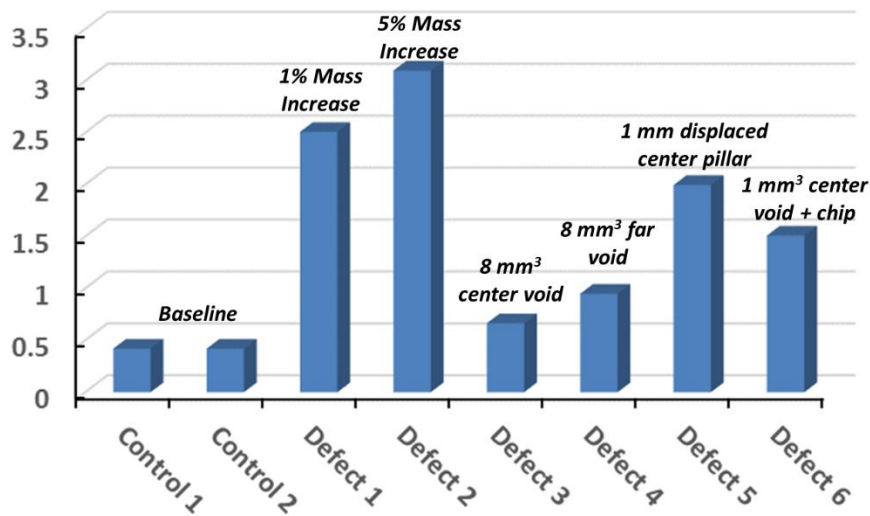
(a) RMSD definition analysis
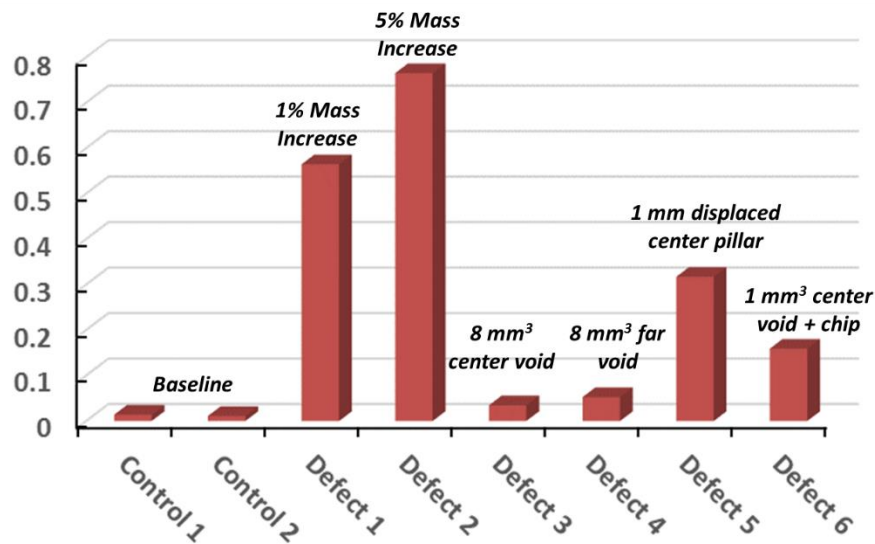
(b) Correlation-based definition analysis

Figure 10. Damage metrics values

However, internal porosity defects (Defects 3 and 4 in Figure 10; Figure 9a-b) have much smaller damage metric values. Therefore, it is possible for these defects to be left undetected, resulting in false-negatives. However, this may be mitigated by interrogating the structure at different frequency ranges that are more sensitive to this type of defect. It is also hypothesized that the damage metrics for these types of defects will be larger when probing a stiffer material such as metal, as it is high resonance.

These results suggest that the proposed technique provides a promising solution quality control as it is able to detect common types of AM defects. Additional work is needed to further investigate the capabilities of this technique and define the sensitivity margins to different types of structural defects.

5. CLOSURE & FUTURE WORK

The lack of suitable Non-destructive Evaluation techniques for qualifying and certifying end-use products fabricated via Additive Manufacturing is seen as a major barrier to the further industrial adoption of AM technologies. Thus, there are several calls for novel NDE techniques that are suitable for accurately analyzing AM parts, which feature complex geometries (e.g., inaccessible features, internal channels, etc.), rough surfaces, and deeply embedded flaws. To address this research gap, the authors propose a NDE technique that employs impedance-based structural monitoring to indirectly measure printed part abnormalities.

To evaluate the feasibility of this novel technique, the authors first designed and fabricated a suite of test parts with representative defects (dimensional inaccuracies, positional inaccuracies, and internal porosities) of AM processes. An impedance-based analysis was conducted on each defected part and then compared with a baseline measurement of a defect-free part. Through this analysis, it was determined that the technique was a feasible means of detecting defects in additively manufactured parts. Specifically, it was demonstrated that the technique could detect print errors in mass (as small as 1%) and in feature displacement (as small as 1mm) of parts created in VeroWhitePlus material. While differences in the damage metrics were identified for the parts featuring 8 mm^3 internal pores, these differences were minimal and could cause the defects to be left undetected.

While feasibility of the approach has been demonstrated, there remain several opportunities for future research. The authors look ahead to quantifying the sensitivity of the approach relative to defect type, size and location, to the relative positions of the defect(s) and sensor, and to the part size and material. As it is hypothesized that the higher stiffness of metal parts would result in even more substantial differences in damage metric, the authors look to conduct additional measurements on directly printed metal parts.

In this paper, the SHM technique is proposed as a post-process NDE approach that would allow for the simple detection of a damage via a go/no-go decision based on the evaluated damage metric. In future work, the authors look to expand the application of this technique as a means of detecting, locating, and quantifying part damage through in-depth analysis of relevant impedance measurements (e.g., machine learning and dynamic part modeling).

6. ACKNOWLEDGMENT

7. REFERENCES

[1] GE Aviation, 2014, "Fit to Print: New Plant Will Assemble World's First Passenger Jet Engine With 3D Printed Fuel Nozzles, Next-Gen Materials," *GE Reports*, http://www.gereports.com/post/80701924024/fit-to-print, June 23.

[2] SpaceX, 2014, "SpaceX Launches 3D-Printed Partto Space, Createse Printed Engine Chamber," http://www.spacex.com/news/2014/07/31/spacex-launches-3d-printed-part-space-creates-printed-engine-chamber-crewed, July 31.

[3] B. Hubscher, 2013, "The Future of Exploration Starts with 3-D Printing," http://www.nasa.gov/exploration/systems/sls/j2x/3d_print.html, March 19.

[4] J. Waller, B. H. Parker, K. L. Hodges, E. R. Burke, and J. L. Walker, 2014, "Nondestructive Evaluation of Additive Manufacturing: State-of-the-Discipline Report," NASA/TM-2014-218560, November.

[5] L. D. Strum, C. B. Williams, J. Camelio, J. White, and R. Parker, 2014, "Cyber-physical Vulnerabilities in Additive Manufacturing Systems," *International Solid Freeform Fabrication Symposium*, Austin, TX., August 4-6.

[6] NIST, 2013, "Measurement Science Roadmap for Metal-based Additive Manufacturing," http://www.nist.gov/el/isd/upload/NISTAdd_Mfg_Report_FINAL-2.pdf, prepared by Energetics Incorporated, May.

[7] ASTM, "Committee F42 on Additive Manufacturing Technologies," http://www.astm.org/COMMITTEE/F42.htm

[8] G. Park, H. Sohn, C. R. Farrar, and D. J. Inman, "Overview of piezoelectric impedance-based health monitoring and path forward," *Shock Vib. Dig.*, vol. 35, no. 6, pp. 451–464, 2003.

[9] C. Liang, F. P. Sun, and C. A. Rogers, "Coupled Electro-Mechanical Analysis of Adaptive Material Systems — Determination of the Actuator Power Consumption and System Energy Transfer," *J. Intell. Mater. Syst. Struct.*, vol. 5, no. 1, pp. 12–20, Jan. 1994.

[10] V. Giurgiutiu and A. N. Zagrai, "Characterization of piezoelectric wafer active sensors," *J. Intell. Mater. Syst. Struct.*, vol. 11, no. 12, pp. 959–976, 2000.

[11] D. J. Leo, *Engineering analysis of smart material systems.* Hoboken, N.J: Wiley, 2007.

[12] J. P. Nokes and G. L. Cloud, "The application of interferometric techniques to the nondestructive inspection of fiber-reinforced materials," *Exp. Mech.*, vol. 33, no. 4, pp. 314–319, Dec. 1993.

[13] D. M. Peairs, P. A. Tarazaga, and D. J. Inman, "Frequency Range Selection for Impedance-Based Structural Health Monitoring," *J. Vib. Acoust.*, vol. 129, no. 6, p. 701, 2007.

[14] G. Park, H. Cudney, and D. Inman, "Impedance-Based Health Monitoring of Civil Structural Components," *J. Infrastruct. Syst.*, vol. 6, no. 4, pp. 153–160, 2000.